

Article

Fatigue Life Improvement of the High Strength Steel Welded Joints by Ultrasonic Impact Peening

Ján Lago ¹, Libor Trško ^{2,*} , Michal Jambor ³, František Nový ³, Otakar Bokůvka ³, Miloš Mičian ³ and Filip Pastorek ²

¹ LAGO Nástrojáreň s. r. o., Veľké Rovné 1571, 013 62 Veľké Rovné, Slovak Republic; lago@lago.sk

² Research centre of the University of Žilina, University of Žilina, Univerzitná 8215/1, 010 26 Žilina, Slovak Republic; filip.pastorek@rc.uniza.sk

³ Faculty of Mechanical Engineering, University of Žilina, Univerzitná 8215/1, 010 26 Žilina, Slovak Republic; michal.jambor@rc.uniza.sk (M.J.); frantisek.novy@fstroj.uniza.sk (F.N.); otakar.bokuvka@fstroj.uniza.sk (O.B.); milos.mician@fstroj.uniza.sk (M.M.)

* Correspondence: libor.trsko@rc.uniza.sk; Tel.: +421-041-513-7629

Received: 13 April 2019; Accepted: 22 May 2019; Published: 28 May 2019



Abstract: Ultrasonic impact peening was applied on welded joints manufactured from Strenx 700 MC high strength low alloy steel with the aim to improve the fatigue properties. Three different surface treatment parameters were tested, which resulted in transformation of the near-surface tensile residual stresses in the weld metal and heat affected zone to compressive residual stress field, while maximal values from -400 MPa up to -800 MPa were reached. The highest fatigue life improvement was reached by the double peening with the 85 N contact force, where the fatigue limit for $N = 10^8$ cycles increased from 370 MPa to 410 MPa.

Keywords: ultrasonic impact peening; high strength low alloy steel; fatigue life; residual stresses; severe plastic deformation

1. Introduction

Welding is still one of the most common methods of joining components in the automotive industry. Since the properties of the welded joints significantly depend on the content of alloying elements, mainly carbon, all the components, which were planned to join in the construction by welding, had to be manufactured from the low-alloyed steels. This fact was for a long time preventing the use of steels with higher mechanical properties to reduce the size and weight of the construction. The weight reduction becomes more important, than it ever was, because of the huge demand for lower fuel consumption, carbon dioxide emission and the higher effectivity of transport (reduction of trailer weight and increase of its loading capacity). These demands caused a strong call for the development of the new types of steels with improved mechanical properties while simultaneously keeping good weldability with common technologies.

Based on these requirements, the steel industry focused on the development of the special high strength low alloy steels (HSLA), which exhibit excellent mechanical properties, while maintaining good weldability with conventional technologies due to their low content of alloying elements. The improvement of mechanical properties is based on special thermo-mechanical processing providing extremely fine-grained microstructures, microstructures strengthened by precipitation hardening or solid solution strengthening [1–4]. The main problem is that the material is locally annealed during the welding, which leads to partial loss of the superior mechanical properties and increases the tendency of the weld for crack initiation during the cyclic loading [5].

Various technologies of application of the cold working processes on the surface of structural materials were developed in recent years and have proven to be very effective for the increase of the fatigue limit of structural materials [6,7]. Those methods are usually based on intensive local plastic deformation of material with an aim to increase the dislocation density (work hardening), accumulate compressive residual stresses and provide grain refinement of the surface layers. One of the intensively studied methods and currently most applied in industry is the shot peening [8–12]. It is performed by bombarding the surface of a component with small spherical shots causing work hardening on the surface, which is performed by a nozzle copying of the component's shape [8]. In the process, the component has to be enclosed inside a cabinet to provide constant peening parameters and to avoid scatter of the media outside of the peening area (avoiding loss of the media, danger to human beings, e. g., the eye contact and breathing of particles and so on). Since the welding is often used on large industrial components and structures, it is impossible to close them inside a cabinet to perform the shot peening process. However, since the welds are the weakest points of the structure and they have just linear trajectories, the complexity of the shot peening process is not so necessary and more direct approach could be applied.

Ultrasonic impact peening (UIP) is a technology of the surface severe plastic deformation using the high velocity impact of a tool, which is exceeded into vibrations at resonance frequency, usually of 20 kHz. It was proven, that with proper peening parameters it is possible to reach similar improvement of mechanical properties as with the more common shot peening process [13–16] and in special cases even improvement in corrosion resistance [17]. However, this technology is not suitable for difficult complex surfaces, though it has a high potential to copy the linear trajectories of welded joints in large constructions, since the peening head requires just the power supply and can be moved freely on the peened surface, while high frequency impact cause intensive plastic deformation of the material localized under the tip of the peening tool. The resulting effect is similar to other methods of surface severe plastic deformation such as shot peening, deep rolling, etc., which is accumulation of compressive residual stresses and grain refinement of the surface layers.

This work describes the results of application of the ultrasonic impact peening process on welded joints manufactured from Strenx 700 MC HSLA steel by the metal active gas (MAG) method. Application of the UIP process with three different process parameters provided changes in the residual stress state of the welded joint and resulted in fatigue life increase in the high-cycle region.

2. Experiment Preparation

2.1. Experimental Material and Weld Execution

Strenx 700 MC is a thermomechanically rolled steel with precisely controlled heating, rolling and cooling process. The chemical composition (Table 1) is characterized by the low carbon and manganese contents to ensure good weldability and precisely added small amounts of elements such as Niobium, Titanium and Vanadium (their summary content cannot exceed 0.22 wt.%) to ensure the grain refinement of the final steel. The grain refinement together with the high micropurity results in the values of ultimate tensile strength (UTS) and the yield point (Table 2), which are usually achieved in low alloy steels after the heat treatment; however, the steel is still suitable for cold forming and welding. According to the EN-10149-2 standard, the EN S700 MC steels rank in the category of extra high strength steels used for various applications, such as the truck frames, cranes and mining machines.

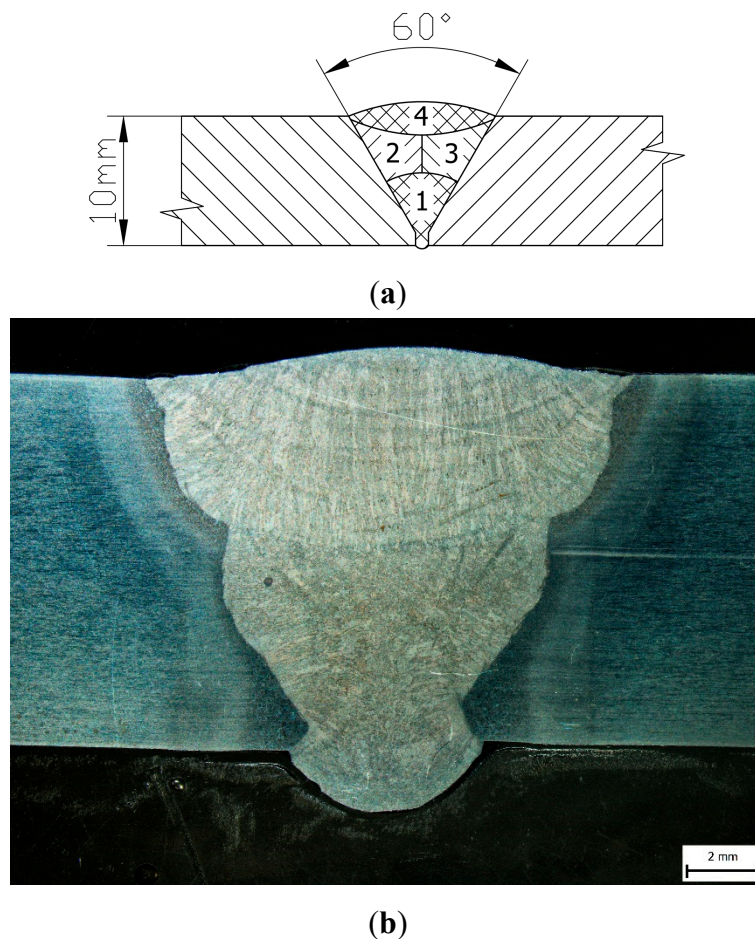
Table 1. Chemical composition of the experimental material Strenx 700 MC (wt.%) obtained by optical emission spectroscopy analysis.

| C | Si | Mn | S | P | Al | Nb | V | Ti | Fe |
|------|-------|------|-------|-------|-------|-------|------|------|-------|
| 0.11 | 0.093 | 0.64 | 0.017 | 0.009 | 0.017 | 0.088 | 0.19 | 0.14 | rest. |

Table 2. Mechanical properties of the Strenx 700 MC obtained by tensile test and Charpy impact test.

| Yield Point [MPa] | UTS [MPa] | Elongation $\delta 5$ [%] | KV [$\text{J}\cdot\text{cm}^{-2}$] | | |
|-------------------|-----------|---------------------------|--------------------------------------|--------|--------|
| | | | +20 °C | −20 °C | −30 °C |
| 741 | 823 | 11.5 | 76 | 51 | 49 |

For experimental works, welded joints manufactured by welding of two 10 mm thick Strenx 700MC sheet metals by the MAG procedure were used. Before the welding, the edges of the sheet metals were machined to a 30° bevel, to create a 60° V shape channel. Welding was carried out with the use of one root bead, two filling beads and one covering bead as sketched in Figure 1. The ESAB OK Aristorod (ESAB, Annapolis Junction, MD, USA) wire was used as a filler material. Its chemical composition and mechanical properties are listed in Table 3 (according to the delivered material datasheet with the wire supply).

**Figure 1.** Welding process of the Strenx 700 MC steel: Sequence of the beads (a), macro-etched cross-section of the final weld (b).**Table 3.** ESAB OK Aristorod 69 chemical composition (wt.%) and mechanical properties.

| C | Si | Mn | Mo | Cr | Ni | V |
|-------------------|------|-----------|------|---------------------------|------|------|
| 0.08 | 0.60 | 1.60 | 0.25 | 0.30 | 1.40 | 0.07 |
| Yield point [MPa] | | UTS [MPa] | | Elongation $\delta 5$ [%] | | |
| 730 | | 800 | | 19 | | |

2.2. Specimens Manufacturing and Surface Strengthening

Specimens for rotating bending fatigue tests with geometry according to Figure 2 were machined in a position where the welded joint was in the middle of the gauge length (Figure 3). Since the rotating bending loading is carried out by symmetrical four-point bending, the loading stress is constant in the gauge length of the specimen [18]. This assures the constant loading value of all the welded joint zones from the weld metal (WM) through the heat affected zone (HAZ) to the base metal (BM) [19]. Specimens in as-welded conditions were ground using the grinding papers up to the #1200, to eliminate the surface roughness created during the specimens machining.

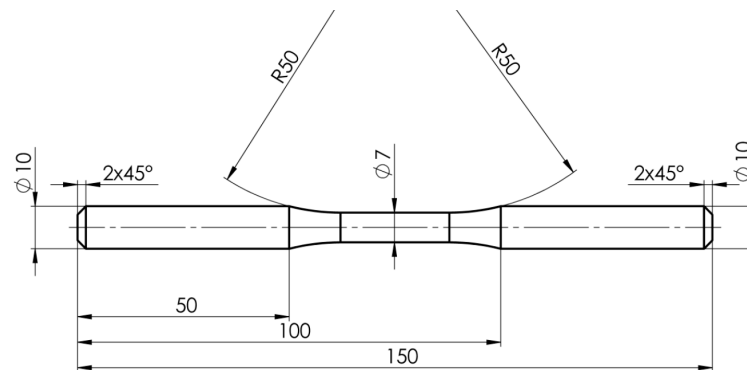


Figure 2. Drawing of the test specimen used for rotating-bending fatigue tests. Dimensions are given in mm.

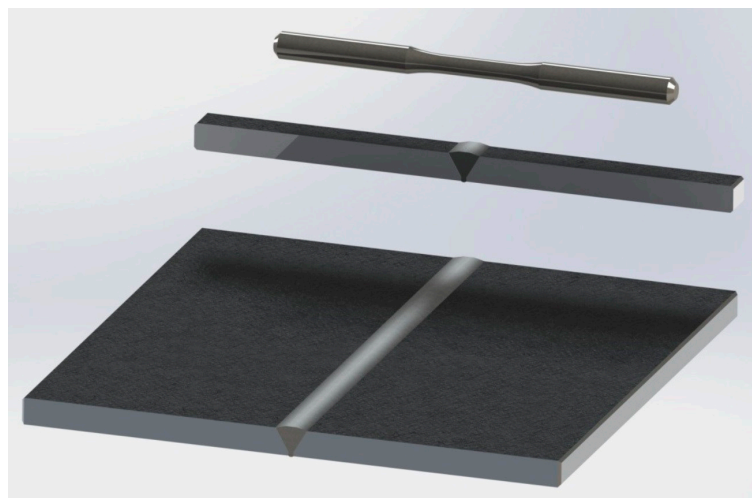


Figure 3. Position of the welded joint in the final rotating-bending fatigue test specimen.

It is important to clarify, that UIP surface treatment was not performed on the as-welded sheet metal material, only on the machined fatigue test specimens.

Surface of the specimens was treated with ultrasonic impact peening technology at impact frequency of $f = 20$ kHz and the displacement amplitude of the contact tip was $\pm 10 \mu\text{m}$ (Figure 4). In the end of the ultrasonic peening tool was inserted a SiC tip with radius of $R = 20$ mm. The tip was sliding on the surface of the specimen and did not perform any relative movement during the peening treatment. Three types of the treatments were carried out. The first treatment was performed at the value of the static contact force of the tool to the specimen of 85 N and the second at 135 N. The third treatment was the double treatment with the contact force of 85 N. The treatment was performed on a lathe (the peening head was mounted in the cutting knife holder). The specimen rotation speed was 720 rpm and main feed was $13.5 \text{ m}\cdot\text{min}^{-1}$, which resulted in the velocity of $15.8 \text{ m}\cdot\text{min}^{-1}$ and

theoretical coverage of ≈ 1500 impact-mm⁻² of the specimen with 7 mm diameter. The contact area was intensively cooled by the flowing metalworking fluid (5% water solution of Emulzin H) throughout the whole ultrasonic peening process, in order to avoid the excessive overheating of the deformed surface.

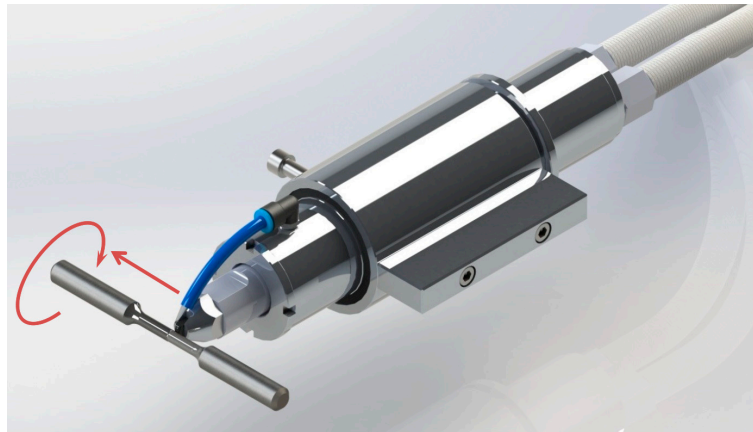


Figure 4. Model of the ultrasonic impact peening process.

3. Results and Discussion

3.1. Basic Mechanical Properties

A welded joint is considered as satisfactory, when its ultimate tensile strength is comparable to the base material. To verify the mechanical properties, two tensile test specimens with 8 mm gauge length diameter, were prepared. This specimen geometry was chosen to be similar to those used for the fatigue tests, thus to verify the mechanical properties of the welded joint in the same conditions in which the fatigue tests were performed. Results of the tensile tests of welded joints (in the as-welded state with polished gauge-length surface) are given in Table 4 and when compared to mechanical properties of the base metal (Table 2), the yield point decreased for approximately 50 MPa, while the UTS value was kept approximately the same. The stress–strain curves (Figure 5) show that the welded material had a significant yield point, which indicates that the welded material kept its ductile properties. The yielding of the test rod 1, in Figure 5, is characterized by two yield points. This is a result of combined microstructures in the welded joint, where the first yielding started at the microstructure with the lowest mechanical properties, probably the weld metal (later confirmed by the hardness test). While the strain hardening mechanism caused increase of the material toughness, the slip was activated in the heat affected zone, where the dislocation density was decreased by annealing during the welding process. Direct correlation with yield points of the original BM and WM cannot be found due to chemical mix and thermal influence of the welding process. For the test rod 2, presented in Figure 5, the described mechanism did not become evident. The elongation of the welded joint is usually higher than of the base metal. This was also confirmed in this case, where the elongation of the welded specimens ($\delta 5 = 12.5\%$) is higher than of the base metal ($\delta 5 = 11.5\%$), however, it is lower than of the filler metal ($\delta 5 = 19\%$). This occurs due to chemical mix and new crystallization of the melted material, which results in combination of the chemical and mechanical properties of the original materials.

Table 4. Results of tensile test, Strenx 700 MC welded joints.

| Specimen | Yield Point [MPa] | UTS [MPa] | Elongation $\delta 5$ [%] |
|----------|-------------------|-----------|---------------------------|
| 1 | 679 | 810 | 12.1 |
| 2 | 684 | 821 | 12.8 |
| Average | 682 | 816 | 12.5 |

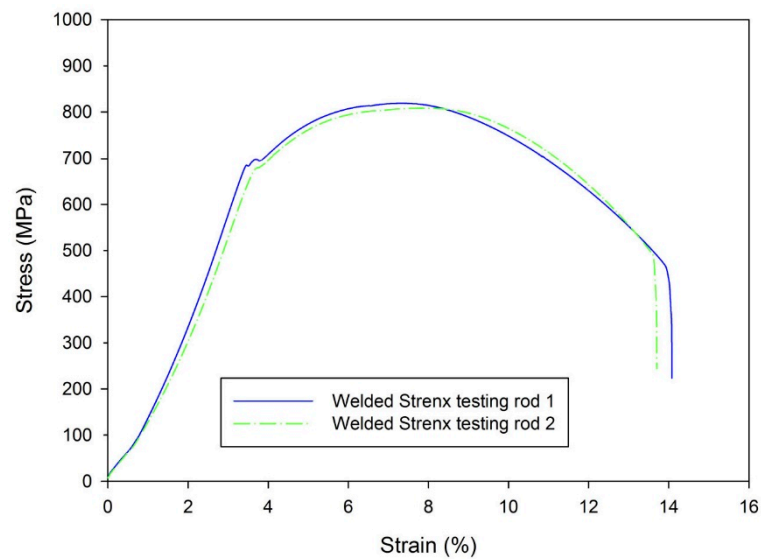


Figure 5. Stress–strain curves of Strenx 700 MC welded joints.

The microhardness measurement (Figure 6) showed that the weld metal and heat affected zone had lower hardness than the base metal. The reason can be found in the fundamental of the Strenx steel manufacturing. To achieve good weldability and high strength, the low alloy steel was thermomechanically processed to obtain a high level of plastic deformation and to decrease the grain size. The melted weld metal in the weld crystallized freely and even when its chemical composition was very similar to the BM, the microstructure was significantly different. Partial recrystallization of the BM occurred in the heat affected zone, which resulted again in decrease of the hardness. This also corresponds to the decrease of the yield point of the welded joint, while keeping the UTS value approximately the same. Since the weld metal was not deformed, it started to yield at much lower force than the BM. However, the weld metal reached the ultimate tensile strength of the BM by significant plastic deformation.

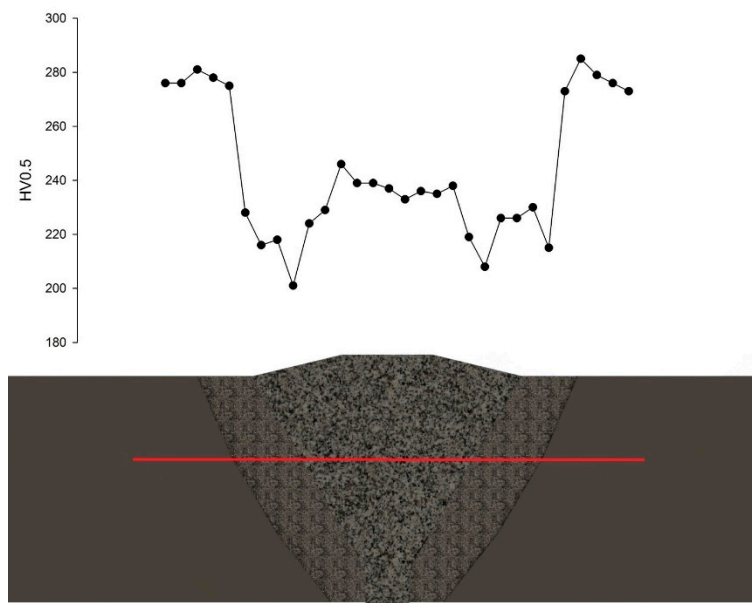


Figure 6. Results of microhardness measurement through the base metal, heat affected zone and weld metal (BM-HAZ-WM) zones of the welded joint.

3.2. Residual Stress Analysis

The residual stresses were analyzed on the final fatigue tests specimens to see the final values after machining and grinding/impact peening. To trace the position of the weld metal and consequently the heat affected area and base metal (Figure 7), the surface of the specimen was etched with 2% Nital. The residual stress measurement was carried out using the Proto iXRD device (Proto, Windsor, ON, Canada), X-ray Cr K α radiation, collimator spot with area of 1 mm², two-peak model and sin² ψ evaluation method [20,21].

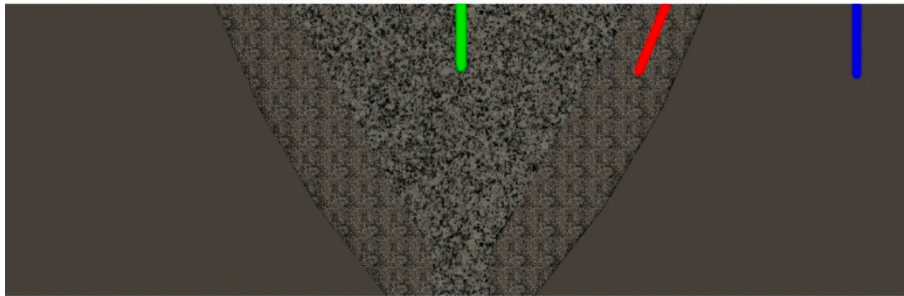


Figure 7. Position of measured residual stresses in the welded joint.

The depth profile residual stress analysis of the sheet metal weld (Figure 8) revealed significant tensile residual stress in the weld metal and heat affected zone, reaching a maximal value of approximately 200 MPa. The base material had typical compressive residual stresses, which are common for the rolled finishing materials.

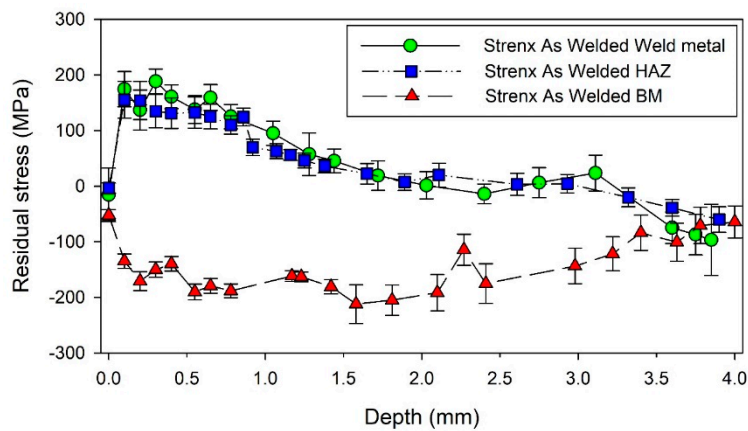


Figure 8. Residual stress in the welded joint zones prior to machining, measured at $\varphi = 0^\circ$ (axial residual stresses).

Since the final specimens were machined and significant layer of material was removed to create the gauge length, another residual stress measurement was carried out to evaluate the residual stresses directly in the machined specimens. As can be seen in Figure 9, machining and grinding created a shallow layer of the compressive residual stresses, approximately 0.1 mm deep. Behind this layer, the values of residual stresses practically copied the character of the curves measured in deeper layers of the original welded joint (Figure 8).

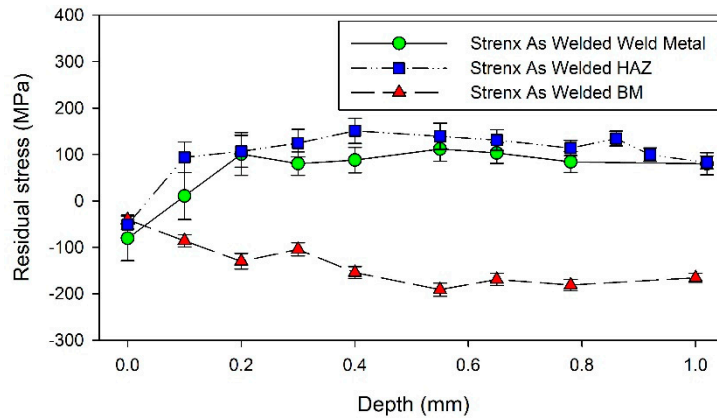
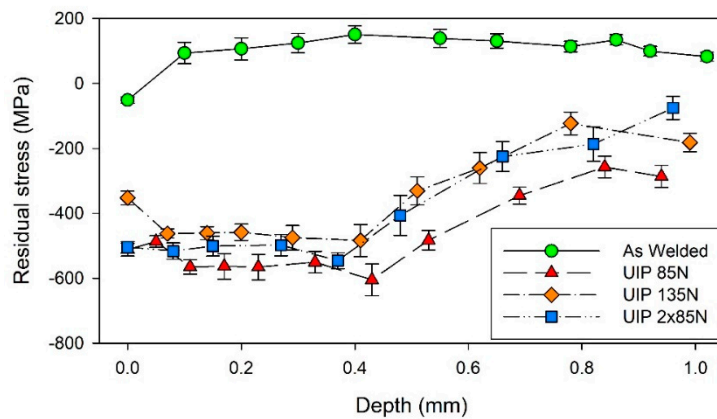
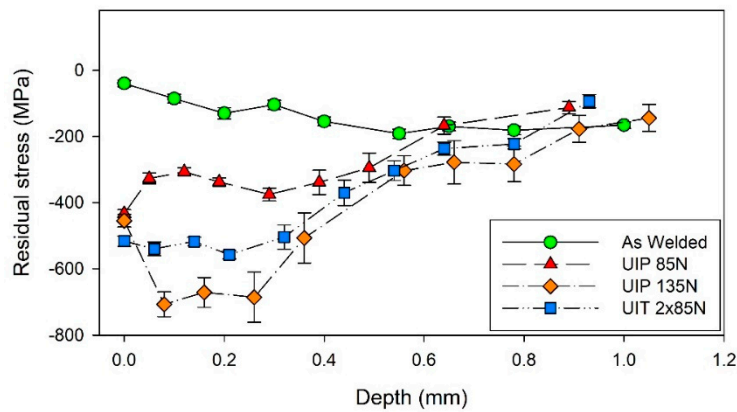


Figure 9. Residual stress in the zones of as welded machined fatigue test specimen, measured at $\varphi = 0^\circ$ (axial residual stresses).

Application of the UIP on the circumference of the fatigue test specimen resulted in transformation of the tensile residual stresses in the weld metal and heat affected zone to high value of compressive residual stresses (Figure 10). The highest values of residual stresses were reached after using the UIP process with 135 N contact force. The effective depth for all the treatment parameters was approximately 1 mm, where the residual stresses converged to the curve of the as-welded material.



(a)



(b)

Figure 10. Cont.

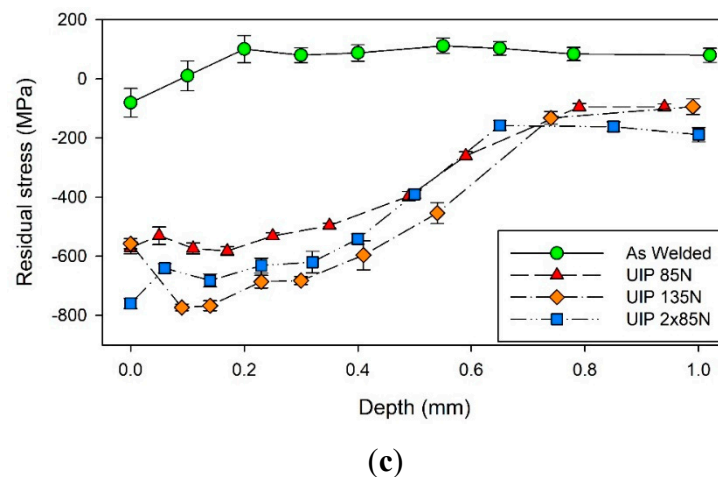


Figure 10. Residual stress in the welded joint zones prior to and after application of the ultrasonic impact peening (UIP) with different parameters, measured at $\varphi = 0^\circ$ (axial residual stresses): WM (a), HAZ (b), BM (c).

3.3. Fatigue Life Results

The fatigue life testing was performed under rotating bending loading with $R = -1$, $f = 20$ Hz and temperature 21 ± 3 °C. Results (Figure 11) show that all the three parameters of the ultrasonic impact peening improved the fatigue properties of the Strenx welded joints. The use of 135 N contact force had only small influence on the fatigue limit, which increased from 370 MPa to 380 MPa at 10^8 run-out number of cycles. However, for lower number of cycles, the fatigue life improvement was significantly higher. For example, for $N = 10^6$ loading cycles, the fatigue strength of the as welded specimens was $N = 385$ MPa and for the UIP 135 N treatment it was 410 MPa. It is necessary to bear in mind, that the scatter of the results for the UIP 135 treatment was high, which assumes an instability of the treatment effect.

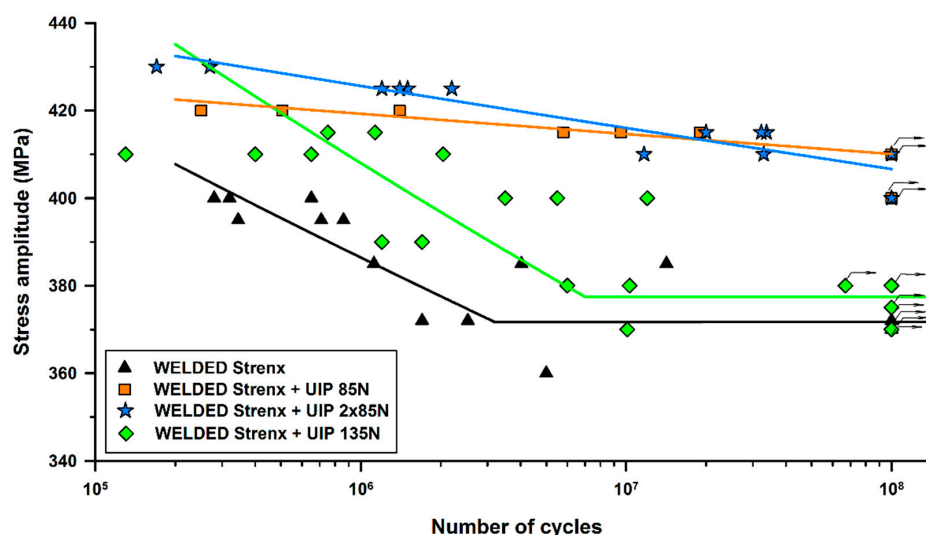


Figure 11. S–N curves of Strenx 700 MC welded joints before and after application of the UIP with different parameters.

Use of treatment with 85 N contact force and double treatment with 85 N contact force (2×85 N) led to significant fatigue life improvement. Both treatments led to increase of the fatigue limit from 370 MPa to 410 MPa. The double treatment with 85 N contact force provided a 10 MPa higher fatigue strength at $N = 10^6$ cycles, when compared to single 85 N treatment.

It seems that the double treatment was more effective in the fatigue life improvement, however the increase of accumulated compressive residual stresses was not very significant. The reason is probably filling of the weaker areas created during the screw-type trajectory of the peening tool on the surface. The trajectory of the second treatment was always axially shifted against the first one, providing the better peening coverage of the surface.

The reason of the drop of fatigue properties after the 135 N contact force treatment was the so-called overpeening effect, usually referred to shot peening process [8,12,22]. Using of too extensive peening parameters caused the increase of the surface roughness and damage of the thin surface layer which accelerated fatigue crack initiation process. This fact is necessary to understand while applying this treatment because the higher intensities, even when they provide the higher residual stresses, do not ensure the highest fatigue properties and fatigue tests are always required.

4. Fracture Surface Analysis

Fracture surfaces of as-welded Strenx 700 MC specimens after fatigue tests were all characterized by the surface fatigue crack initiation (Figure 12a,b) in the HAZ. In the area of stable fatigue crack growth, the propagation was mostly realized by transcrystalline fatigue mechanism and a local presence of secondary cracks and facets of intercrystalline fracture appeared (Figure 12c). The final fracture had a character of transcrystalline ductile fracture with dimple morphology.

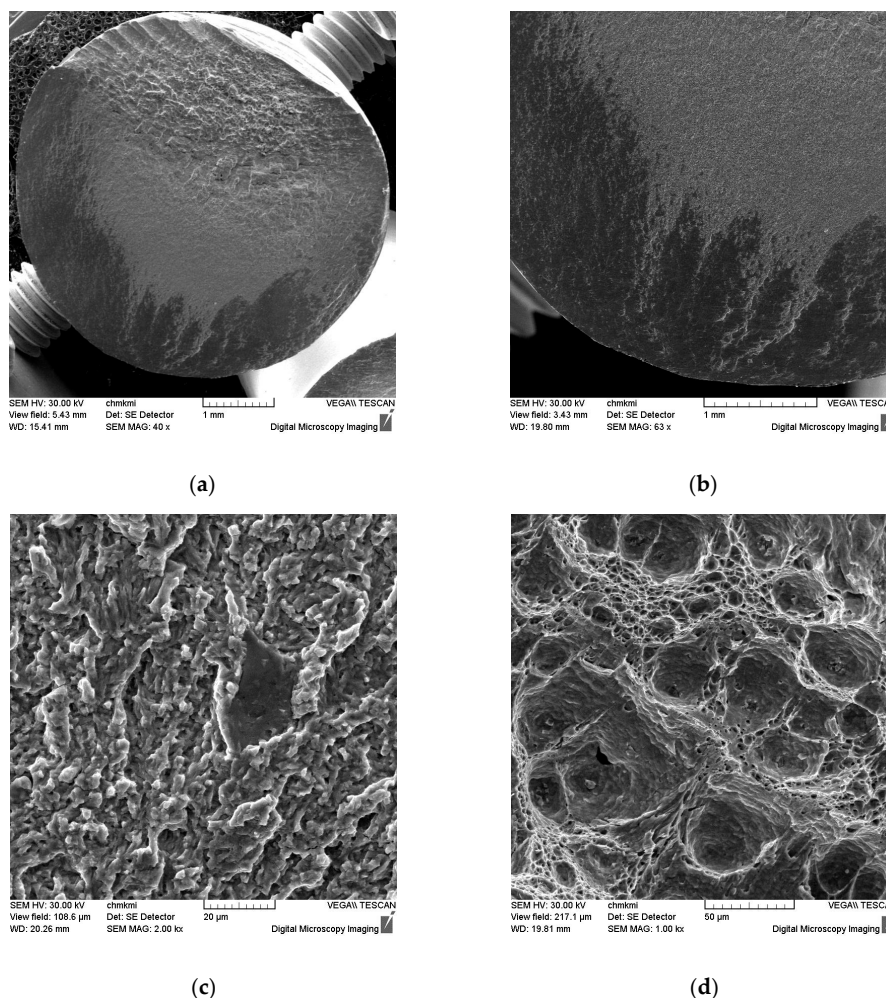


Figure 12. Fracture surface of as-welded Strenx 700 MC specimen loaded at 395 MPa and fractured after 6.86×10^5 cycles: Overall view of the fracture (a), detail of surface fatigue crack initiation (b), fatigue crack propagation with intercrystalline facet (c) and final fracture (d).

Fatigue crack in the specimens treated by the UIP initiated always in the HAZ. Surface treatment with the UIP process shifted the fatigue crack initiation into the subsurface of the material, mostly on various welding defects such as pores and large inclusions. Figure 13a shows the fracture surface of the UIP 85N specimen where the fatigue crack was initiated by the “fish-eye” mechanism. In this case, the crack initiated and propagated around the defect creating so called “optically dark area” (Figure 13b). When the inner crack reached the surface of the specimen, the crack started to propagate by typical transcrystalline fatigue mechanism. The delamination of the strengthened surface layer can be observed in the near-surface area of the fracture surface (Figure 13c). The strengthened surface also created an area with finer transcrystalline dimples in the area of final fracture (Figure 13d).

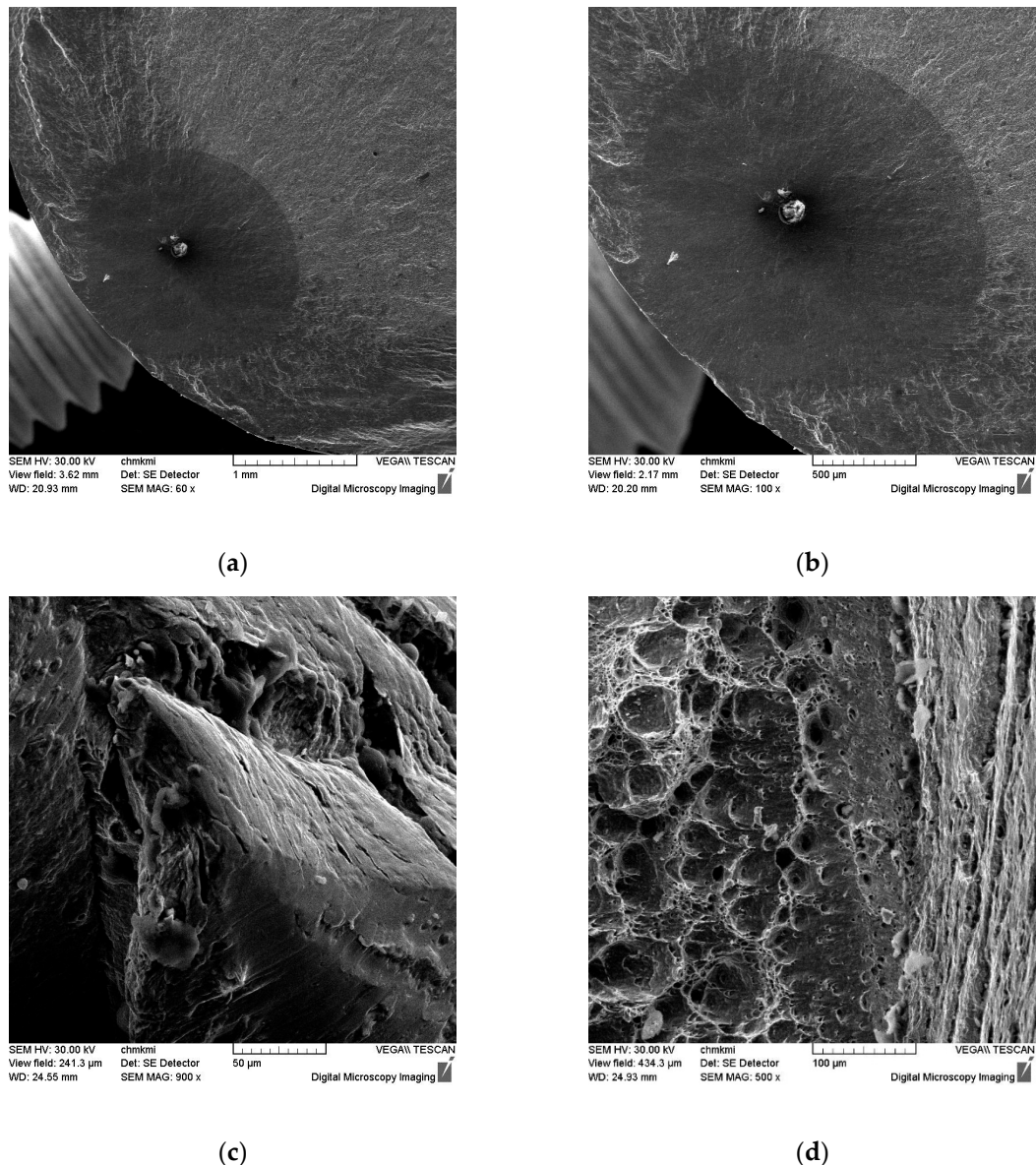


Figure 13. Fracture surface of UIP 85N Strenx 700 MC specimen loaded at 415 MPa and fractured after 5.8×10^6 cycles: Overall view of the fracture (a), detail of fish-eye fatigue crack initiation (b), delamination of the strengthened surface layer (c) and final fracture with area of finer dimples in the strengthened surface layer (d).

Subsurface fatigue crack initiation and delamination of the strengthened surface layer was also common for all the UIP 2 × 85 N (Figure 14) and UIP 135 N (Figure 15) specimens. Since the UIP process affects only the surface layer, the fatigue crack propagation mechanism and mechanism of final

fracture were identical in all specimens, thus transcrystalline fatigue mechanism with local occurrence of intercrystalline facets and transcrystalline ductile fracture with dimple morphology respectively.

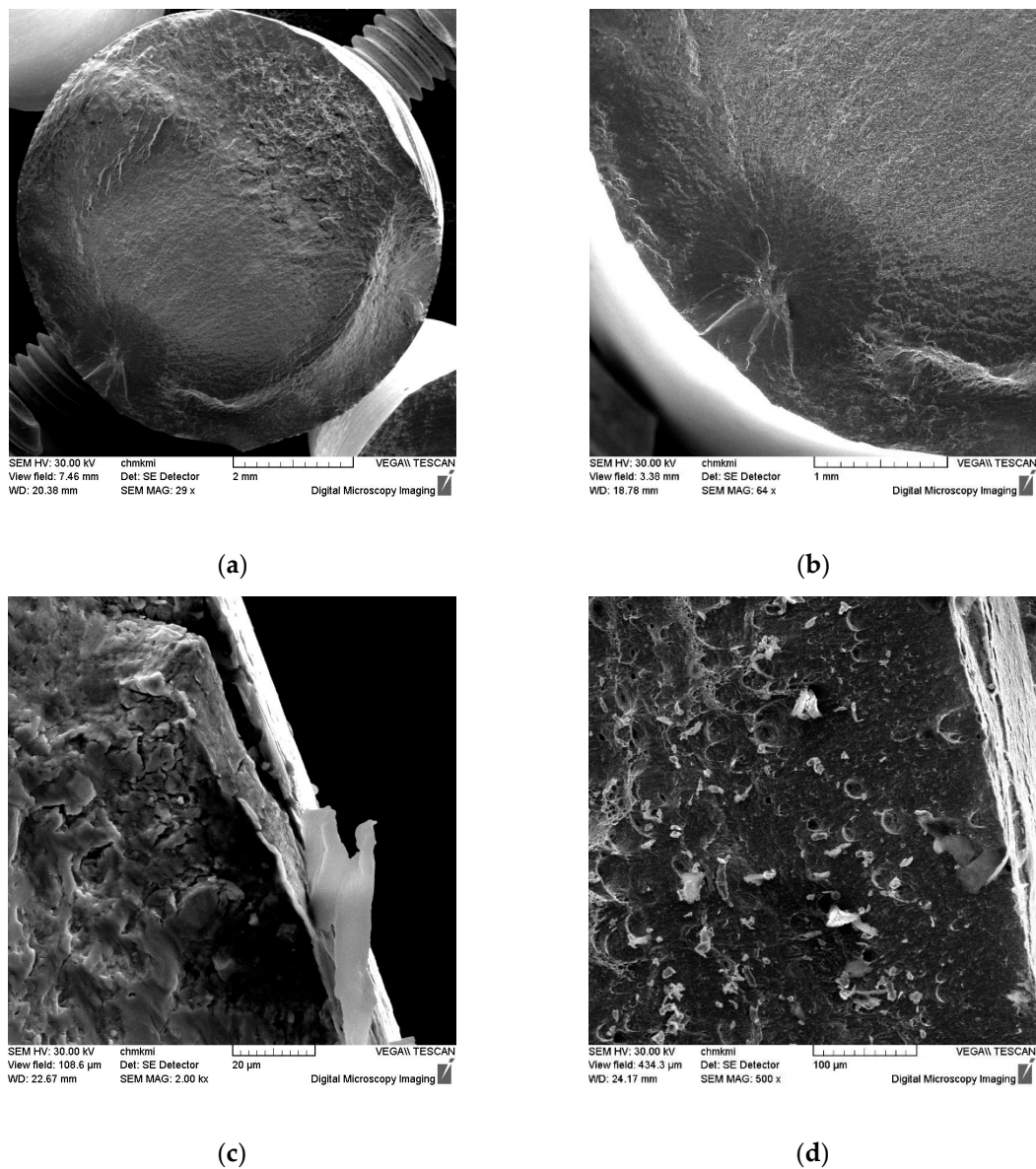


Figure 14. Fracture surface of UIP 2 × 85 N Strenx 700 MC specimen loaded at 415 MPa and fractured after 3.23×10^7 cycles: Overall view of the fracture (a), detail of fish-eye fatigue crack initiation (b), delamination of the strengthened surface layer (c) and final fracture with area of finer dimples in the strengthened surface layer (d).

The fact that the fatigue crack always initiated in the HAZ shows, that this zone was the weakest point of the welded joint in terms of cyclic loading. The shift of the fatigue crack initiation point to subsurface volumes of material was caused by an increase of the dislocation density in the treated surface layer. Further dislocation slip (micro-plastic deformation), which is necessary for the fatigue crack nucleation process, is limited in the microstructure with near-saturated dislocation density. In this case, even when the loading stress in the subsurface volume was lower than the nominal loading stress on the surface (resulting from the character of the rotating bending loading, where the maximal stress is on the surface and reaches zero in the specimen's axis), microstructural defects such as pores and intermetallic inclusions took place as the points with higher stress concentration. This effect is a result

of high-quality and uniform surface treatment, with no under-treated (weak spots) or over-treated (surface delamination) surface areas, which would serve as stress concentrators.

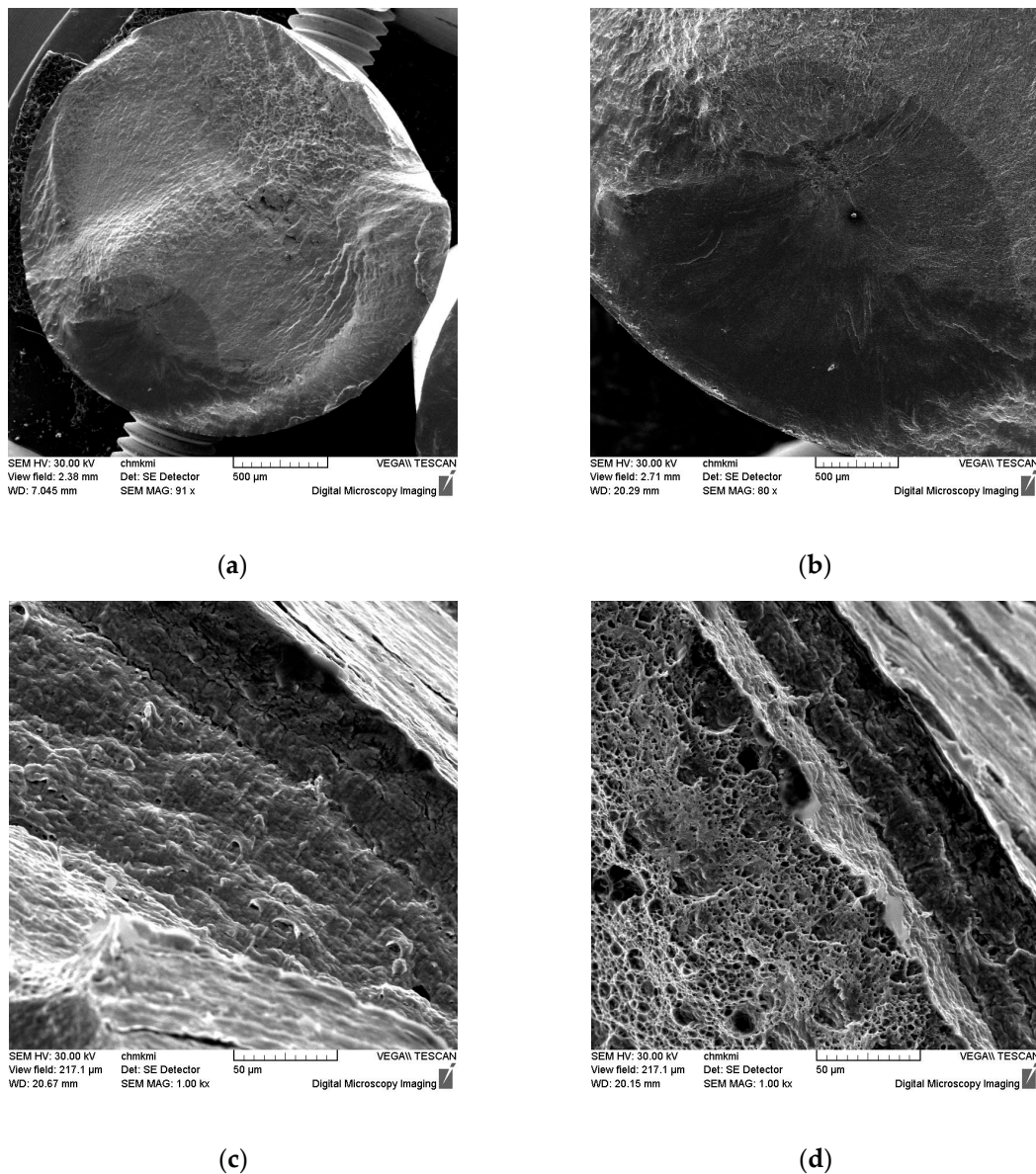


Figure 15. Fracture surface of UIP 135 N Strenx 700 MC specimen loaded at 410 MPa and fractured after 4.0×10^5 cycles: Overall view of the fracture (a), detail of fish-eye fatigue crack initiation (b), ductile delamination of the strengthened surface layer (c) and final fracture with area of finer dimples in the strengthened surface layer (d).

5. Conclusions

Based on the experimental results, the following can be concluded:

- Joining of Strenx 700 MC steel with OK Aristorod 69 welding wire created a joint with similar ultimate tensile strength, however the yield point decreased for approx. 50 MPa.
- The welding process caused accumulation of tensile residual stresses in the weld metal and heat affected zone, which reached maximal value of approximately 200 MPa.
- The ultrasonic impact peening (UIP) was able to transform the tensile residual stresses in the weld metal and heat affected zone into compressive ones, with maximal values between -400 and -800 MPa.

- Increasing of severity of the ultrasonic impact peening increased the values of residual stresses correspondingly.
- The highest fatigue life improvement was reached by the double peening with the 85 N contact force, where the fatigue limit for $N = 10^8$ cycles increased from 370 MPa to 410 MPa, while the S–N curve in the region of the lower number of cycles to failure was approx. 10 MPa above the single treatment with 85 N contact force.
- Since the fatigue crack always initiated in the HAZ, this area can be considered as the weakest point of the welded joint in terms of cyclic loading.
- Treatment with the UIP process caused shifting of the fatigue crack initiation point from the surface to the sub-surface volume of material, where weld defects acted as the most significant stress concentrators.

Author Contributions: Experiment design and surface treatment (J.L.), residual stress evaluation (L.T.), fatigue testing (M.J.), mechanical testing (F.N., F.P.), data evaluation (O.B.), welding (M.M.).

Funding: This research was funded by APVV, grant number APVV-16-0276; VEGA, grant number 1/0951/17 and KEGA, grant number 009ŽU-4/2019.

Conflicts of Interest: The authors declare no conflict of interest.

References

1. Shao, Y.; Liu, C.; Yan, Z.; Li, H.; Liu, Y. Formation mechanism and control methods of acicular ferrite in HSLA steels: A review. *J. Mater. Sci. Technol.* **2018**, *34*, 737–744. [[CrossRef](#)]
2. Park, D.B.; Huh, M.Y.; Shim, J.H.; Suh, J.Y.; Lee, K.H.; Jung, W.S. Strengthening mechanism of hot rolled Ti and Nb microalloyed HSLA steels containing Mo and W with various coiling temperature. *J. Mater. Sci. Eng. A* **2013**, *560*, 528–534. [[CrossRef](#)]
3. Bakkaloğlu, A. Effect of processing parameters on the microstructure and properties of an Nb microalloyed steel. *Mater. Lett.* **2002**, *56*, 263–272. [[CrossRef](#)]
4. Charleux, M.; Poole, W.J.; Militzer, M.; Deschamps, A. Precipitation behavior and its effect on strengthening of an HSLA-Nb/Ti steel. *Metall. Mater. Trans. A* **2001**, *32*, 1635–1647. [[CrossRef](#)]
5. Jesus Jorge, J.; Cândido, V.S.; Rios da Silva, A.C.; Costa Garcia Filho, F.; Camoso Pereira, A.; Santos da Luz, F.; Neves Monteiro, S. Mechanical properties and microstructure of SMAW welded and thermally treated HSLA-80 steel. *J. Mater. Res. Technol.* **2018**, *7*, 598–605. [[CrossRef](#)]
6. Lu, J.; Lu, K. Surface nanocrystallization (SNC) of materials and its effect on mechanical behavior. *Comp. Struct. Int.* **2003**, *8*, 495–528.
7. Lu, K.; Lu, J. Surface nanocrystallization (SNC) of metallic materials—presentation of the concept behind a new approach. *J. Mater. Sci. Technol.* **1999**, *15*, 193–197.
8. Abadie, F.X.; Beckmerhagen, P.; Belassel, M. *Shot peening: A Dynamic Application and its Future*, 3rd ed.; Metal Finishing News: Wetzikon, Switzerland, 2009; pp. 17–44.
9. Bagheri, S.; Guagliano, M. Review of shot peening processes to obtain nanocrystalline surfaces in metal alloys. *Surf. Eng.* **2009**, *25*, 3–14. [[CrossRef](#)]
10. Bagherifard, S.; Guagliano, M. Fatigue behavior of a low alloy steel with nanostructured surface obtained by severe shot peening. *Eng. Fract. Mech.* **2012**, *81*, 56–68. [[CrossRef](#)]
11. Trško, L.; Bokůvka, O.; Nový, F.; Guagliano, M. Effect of severe shot peening on ultra-high-cycle fatigue of a low-alloy steel. *Mat. Des.* **2014**, *57*, 103–113. [[CrossRef](#)]
12. Trško, L.; Guagliano, M.; Bokůvka, O.; Nový, F.; Jambor, M.; Florková, Z. Influence of Severe Shot Peening on the Surface State and Ultra-High-Cycle Fatigue Behavior of an AW 7075 Aluminum Alloy. *J. Mater. Eng. Perform.* **2017**, *26*. [[CrossRef](#)]
13. Cao, X.J.; Pyoun, Y.S.; Murakami, R. Fatigue properties of a S45C steel subjected to ultrasonic nanocrystal surface modification. *Appl. Surf. Sci.* **2010**, *256*, 6297–6303. [[CrossRef](#)]
14. Liu, J.; Suslov, S.; Vellore, A.; Ren, Z.; Amanov, A.; Pyun, Y.S.; Martini, A.; Dong, Y.; Ye, C. Surface nanocrystallization by ultrasonic nano-crystal surface modification and its effect on gas nitriding of Ti6Al4V alloy. *J. Mater. Sci. Eng. A* **2018**, *736*, 335–343. [[CrossRef](#)]

15. Tsai, W.Y.; Huang, J.C.; Gao, Y.J.; Chung, Y.L.; Huang, G.R. Relationship between microstructure and properties for ultrasonic surface mechanical attrition treatment. *Script. Mater.* **2015**, *103*, 45–48. [[CrossRef](#)]
16. Zhou, J.; Sun, Z.; Kanouté, P.; Reiraint, D. Effect of surface mechanical attrition treatment on low cycle fatigue properties of an austenitic stainless steel. *Int. J. Fatigue* **2017**, *103*, 309–317. [[CrossRef](#)]
17. Dong, Z.; Liu, Z.; Li, M.; Luo, J.L.; Chen, W.; Zheng, W.; Guzonas, D. Effect of ultrasonic impact peening on the corrosion of ferritic–martensitic steels in supercritical water. *J. Nucl. Mater.* **2015**, *457*, 266–272. [[CrossRef](#)]
18. Bokůvka, O.; Nicoletto, G.; Guagliano, M.; Kunz, L.; Palcek, P.; Novy, F.; Chalupova, M. *Fatigue of Materials at Low and High Frequency Loading*, 2nd ed.; University of Zilina: Zilina, Slovakia, 2015; ISBN 978-80-554-0857-6.
19. Lago, J.; Guagliano, M.; Bokůvka, O.; Trško, L.; Řidký, O.; Nový, F.; Závodská, D. Improvement of fatigue endurance of welded S355 J2 structural steel by severe shot peening. *Surf. Eng.* **2017**, *33*, 715–720. [[CrossRef](#)]
20. Noyan, I.C.; Cohen, J.B. *Residual Stress-Measurement by Diffraction and Interpretation*; Springer: New York, NY, USA, 1987.
21. Fitzpatrick, M.E.; Fry, A.T.; Holdway, P.; Kandil, F.A.; Shackleton, J.; Suominen, L. *Determination of Residual Stresses by X-ray Diffraction*, 2nd ed.; National Physical Laboratory: Teddington, UK, 2005; pp. 42–48.
22. Trško, L.; Fintová, S.; Nový, F.; Bokůvka, O.; Jambor, M.; Filip, P.; Florková, Z.; Oravcová, M. Study of Relation between Shot Peening Parameters and Fatigue Fracture Surface Character of an AW 7075 Aluminium Alloy. *Metals* **2018**, *8*, 111. [[CrossRef](#)]



© 2019 by the authors. Licensee MDPI, Basel, Switzerland. This article is an open access article distributed under the terms and conditions of the Creative Commons Attribution (CC BY) license (<http://creativecommons.org/licenses/by/4.0/>).